AGU PUBLICATIONS

Geophysical Research Letters

RESEARCH LETTER
10.1002/2015GL065100

Key Points:
- CO_2 injection in tight shale effectively produces oil without fracturing the formation
- Positron emission tomography successfully used to explicitly image CO_2 flow in shale
- Diffusion coefficient derived exclusively from PET imaging in fractured media during CO_2 injection

Correspondence to:
M. A. Fernø,
Martin.Ferno@uib.no

Citation:
Fernø, M. A., L. P. Hauge, A. Uno Rognmo, J. Gauteplass, and A. Graue (2015), Flow visualization of CO_2 in tight shale formations at reservoir conditions, *Geophys. Res. Lett.*, *42*, 7414–7419, doi:10.1002/2015GL065100.

Received 6 JUL 2015
Accepted 25 AUG 2015
Accepted article online 29 AUG 2015
Published online 18 SEP 2015

Flow visualization of CO_2 in tight shale formations at reservoir conditions

M. A. Fernø[1], L. P. Hauge[1], A. Uno Rognmo[1], J. Gauteplass[1], and A. Graue[1]

[1]Department of Physics and Technology, University of Bergen, Bergen, Norway

Abstract The flow of CO_2 in porous media is fundamental to many engineering applications and geophysical processes. Yet detailed CO_2 flow visualization remains challenging. We address this problem via positron emission tomography using ^{11}C nuclides and apply it to tight formations—a difficult but relevant rock type to investigate. The results represent an important technical advancement for visualization and quantification of flow properties in ultratight rocks and allowed us to observe that local rock structure in a layered, reservoir shale ($K = 0.74$ μdarcy) sample dictated the CO_2 flow path by the presence of high-density layers. Diffusive transport of CO_2 in a fractured sample (high-permeable sandstone) was also visualized, and an effective diffusion coefficient ($D_i = 2.2 \cdot 10^{-8}$ m^2/s) was derived directly from the dynamic distribution of CO_2. During CO_2 injection tests for oil recovery from a reservoir shale sample we observed a recovery factor of $R_F = 55\%$ of oil in place without fracturing the sample.

1. Introduction

Easily accessible energy sources are a prerequisite for a sustainable future for human kind. Synergy between the need for increased energy production and the needed reduction in anthropogenic CO_2 emissions has been suggested through CO_2 storage in mature oil fields, with associated incremental oil recovery [see, e.g., *Falcone and Harrison*, 2013]. This approach has been termed carbon capture *utilization* and storage (CCUS) where CO_2 emissions from energy production are captured and injected into the subsurface to reduce the carbon footprint associated with fossil fuels in a transitional phase to a more sustainable energy outlook [*Chu and Majumdar*, 2012]. Specifically for CCUS, research on transport and trapping mechanisms in storage sites is needed to minimize costs and ensure safe long-term CO_2 storage.

1.1. Oil Recovery and Diffusivity in Shales

Shale formations are considered impermeable layers that restrict upward migration of hydrocarbons and CO_2 in sedimentary formations in the subsurface [*Eiken et al.*, 2011]. Recently, shale has also become a target for hydrocarbon exploration and is rapidly becoming a major energy resource worldwide but especially true in the U.S. Economic hydrocarbon production from such reserves was until recently unfeasible mainly related to the very low to ultralow rock permeability, a parameter that determines the connectivity and flow between pores where hydrocarbons are stored. Harvesting the energy stored in a shale formation today relies on creating conduits for flow through high-pressure injection of water to hydraulically fracture the near-well regions. Although hitherto a major economic success, using data from 65,000 shale wells in 30 shale gas and 21 tight oil fields in the U.S., Hughes argued that the shale revolution will be hard to sustain because well production rates decline rapidly within a few years [*Hughes*, 2013]. Indeed, production generally falls as the square root of time, indicative of diffusive drive [*Patzek et al.*, 2013]. Molecular diffusion is the mixing of fluids due to random motion of molecules and can be expressed by the following equation derived from Fick's second law of diffusion in bulk fluids:

$$C_i = C_0\left(1 - \mathrm{erf}\left(\frac{x}{2\sqrt{D_i t}}\right)\right) \quad (1)$$

where C_i is the concentration of phase i, C_0 is the surface concentration, t is time, x is distance, and D_i is the molecular diffusion coefficient. Diffusion lengths are determined by tortuosity and are generally longer in porous media compared with bulk systems. Effective diffusion coefficients based on Fickian diffusion may not apply in ultratight formations [*Webb and Pruess*, 2003], although the error introduced by using an incorrect diffusion model decreases at elevated pressures. We reserve a full investigation of diffusive

models in shale samples for future work and use here a fractured sandstone core rather than a shale sample as we here wish to emphasize the use of local CO_2 tracking in the determination of D_i.

1.2. CO_2 Injection for Oil Recovery in Tight Shales

Current production behavior from fractured, tight gas reserves suggests a diffusive drive and similar behavior is expected in tight oil formations during CO_2 injection. Although steeply declining production rates and low overall recoveries are observed in shale formations—largely a result from challenging microscopic characteristics such as pore sizes (in the nanometer range), pore connectivity (permeability in microdarcy to nanodarcy range), and surface properties of the rock (to a large degree unknown)—the number of scientific investigations into the underlying mechanisms is still low. Other possible fracking fluids exist, but water is cheap and (still) readily available, so a switch is unlikely before the increased costs of other fluids are justified or policies are changed. Advantages using CO_2 as a fracking fluid were recently discussed by *Middleton et al.* [2015], in which large volumes of CO_2 could be used for energy production from shale, combined with a significant reduction of water usage for fracturing and large-scale storage of CO_2. Specifically, improved CO_2 technology must be developed through research on transport and trapping mechanisms in storage sites to minimize costs and ensure safe long-term CO_2 storage. Indeed, improved knowledge about flow in unconventional rocks also provides the necessary basis to improve current production rates. In this context, access to detailed flow information is vital. Reactivity between dry supercritical CO_2 and the shale is generally low but may potentially extract organic matter [*Busch et al.*, 2008] and may be a beneficial, combined effect during CO_2 injection for fracking as suggested by others [see, e.g., *Middleton et al.*, 2015] for CCUS. The oil recovery in oil-bearing U.S. shale reservoirs like the Bakken or Eagleford formation is believed to be less than 10%, and the potential for enhanced oil recovery (EOR) is therefore huge. We present the first CCUS experimental results of explicit CO_2 flow visualization in porous media using positron emission tomography (PET) and report high oil recoveries during CO_2 injection using samples from an oil-producing unit in the U.S. We also use the CO_2 tracking data to gain insight to local flows in a layered shale sample and to calculate a diffusion coefficient directly from visualization data in a fractured sandstone core to demonstrate the use of a new imaging tool for explicit CO_2 flow tracking in unconventional and fractured formations.

2. Materials and Methods

2.1. Positron Emission Tomography (PET)

Although primarily used as a clinical diagnostic tool, PET has previously been used to visualize fluids in porous structures [see, e.g., *Boutchko et al.*, 2012; *Kulenkampff et al.*, 2008]. PET is based on positron-emitting radionuclides where a positron is emitted from the nucleus accompanied by an electron to balance atomic charge. The positron loses kinetic energy by interactions with the surroundings, and at near-zero momentum the positron combines with an electron and annihilates. The physics of nucleus decay and annihilation limits the spatial resolution of PET, and the achieved resolution depends on the distance to the detectors. A detector array registers the electromagnetic radiation in the form of two 511 keV photons emitted in opposite directions to conserve momentum. For practical purposes, the beta decay is insensitive to temperature and pressure [*Emery*, 1972], which, combined with high photon energy, makes making PET particularly suitable for visualization of flow in porous rocks because the photons penetrate the aluminum confinement vessel holding the rock sample at elevated pressures.

Throughout this article, we will also use the phrase *explicit* imaging when discussing PET imaging. We use the term explicit imaging to emphasize that PET provides a direct measurement of the labeled fluid saturation, which is CO_2 in this work. In contrast, attenuation methods, such as X-ray and the more common computed tomography (CT), measure fluid saturation indirectly, through the gradual loss in X-ray flux intensity through the medium that produces a time-averaged density distribution image of the rock, if fluids with sufficient density difference are used. Comparison and use of PET and CT for flow visualization in porous rocks is detailed elsewhere [*Fernø et al.*, 2015].

2.2. Experimental Setup for CO_2 Injection and Explicit CO_2 Tracking

Cylindrical core plugs were installed in an aluminum biaxial core holder (*CoreLab Hassler Core Holder*) with a rubber sleeve to apply a radial confinement pressure to ensure that the injected fluid was transported through the pore space. The core holder with the rock samples was placed in the center of the PET/CT (*Siemens Biograph Truepoint PET-CT*) bore (diameter 700 mm). A CT image (voxel size 0.156 mm^3:

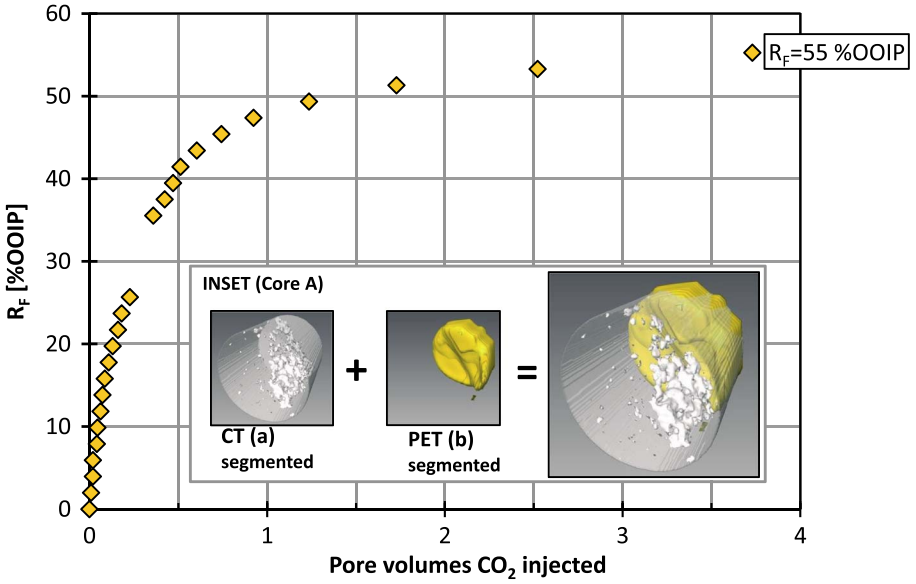

Figure 1. Oil recovery by CO_2 injection in ultratight unconventional stacked core system. Graph: Average oil recovery versus time (pore volumes injected) resulting in final oil recovery of 55% OOIP during 3.7 PV CO_2 injected using Cores A, B, and C. Inset: Visualization of rock characteristics through CT imaging (grey scale), coupled with explicit CO_2 signal through PET imaging in Core A. Aligning a threshold CT image (i) and CO_2 PET image (ii), obtained after 1 h injection, we observe that the emerged CO_2 flow pattern correlated to local rock structure and layered high-low density bands. The injected CO_2 flowed in the lower density regions of the core sample, indicative of a layered permeability system, leading to viscous fingers and a highly irregular displacement front.

$0.51 \times 0.51 \times 0.6\ mm^3$) was obtained to ensure that the rock sample was positioned correctly in the PET detector array and adjusted if needed. Unlike normal diagnostic operations, the rock system was stationary positioned within detector array, with an axial field of view of 169 mm. This allowed for dynamic scans with extended PET recording times (up to 17 h continuous scanning was successfully tested) with a spatial voxel size of $8.49\ mm^3$ ($2.04 \times 2.04 \times 2.04\ mm^3$). Signals were continuously recorded, and temporal resolution was set during postprocessing and determined based on a balance between image quality, expressed as signal-to-noise ratio (SNR), and temporal resolution: the higher temporal resolution (shorter time between each image), the lower SNR. An excellent SNR of 200:1 was achieved using temporal resolutions of 10–30 s.

Positron-emitting radionuclides were produced using particle accelerators on site due to the relatively short half-life (approximately 20 min). Reduction in signal intensity by radioactive decay during flow tests was correctly compensated for using algorithms imbedded in the standard PET/CT software provided by the manufacturer. The use of ^{11}C as a radionuclide tag for methane (CH_4) has previously been proposed [*Maucec*, 2013] but experimentally verified in this work, for the first time, to characterize CO_2 flow in porous systems. The $^{11}CO_2$ phase was produced in a cyclotron by bombarding the target media ($N_2 + 1\%\ O_2$) with 16.5 MeV protons. A batch of 78 ml $^{11}CO_2$ (and traces of nitrogen) was mixed with CO_2 in a $1\ dm^3$ injection pump (*ST Stigma 1000*) and pressurized to experimental conditions. Each injection test started approximately one half-life after initial ^{11}C delivery. Injected radioactive CO_2 was collected at the outlet in a production pump set to maintain a constant pressure.

3. Experimental Results and Discussion

3.1. Description of CO_2 Flow and CO_2 EOR in Tight Shale

With nanodarcy level permeability, properties like effective diffusion coefficients, CO_2 capillary entry pressure, and CO_2 flow description in the shale are generally very difficult to measure accurately in the laboratory [*Liu et al.*, 2012]. In this context, alternative approaches to measure these properties are useful, and we report here the first experimental demonstration of CO_2 tracking for flow characterization in shale using PET/CT imaging. We also evaluate the oil recovery by CO_2 injection (see Figure 1), without fracking,

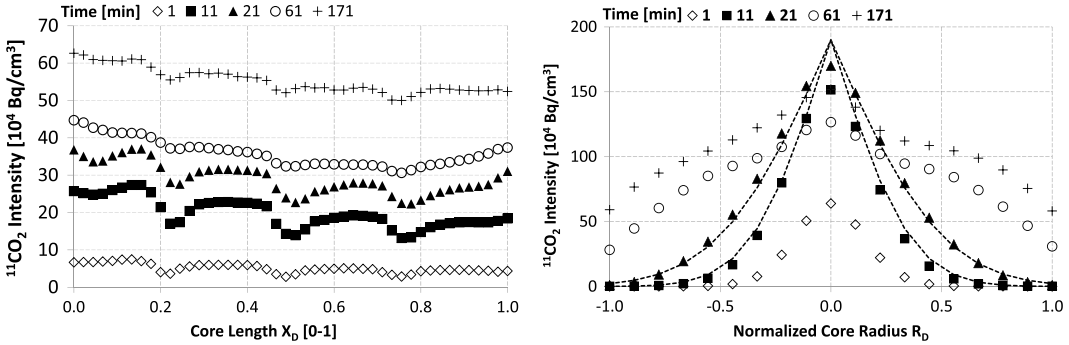

Figure 2. Visualization of diffusive CO_2 transport and mixing in a fractured (1 mm constant fracture aperture held open with a spacer) oil-saturated (n-decane) Bentheim core plug. (left) Dynamic longitudinal $^{11}CO_2$ profiles showing increased CO_2 saturation over time. Slight intensity dips along the length correlate to support columns in spacer. (right) Symmetric, transverse diffusive CO_2 transport from the CO_2 saturated fracture ($R_D = 0.0$) into the oil-saturated matrix at location $X_D = 0.5$. Analytical profiles (dashed lines) using equation (1) were fitted to dynamic imaging data with an effective diffusion coefficient of $2.2 \cdot 10^{-8}$ m^2/s.

in ultratight, unconventional shale core plugs using three stacked 1.5 in diameter cores (*Core A*: $K = 0.74$ μdarcy, $L = 3.92$ cm; *Core B*: $K = 1.7$ μdarcy, $L = 3.80$ cm; *Core C*: $K = 0.12$ μdarcy, $L = 2.45$ cm). Injection conditions ($\Delta P = 7.09$ MPa; $P_{inlet} = 22.1$ MPa and $P_{outlet} = 15.0$ MPa; $T = 60$°C) were above minimum miscibility pressure (MMP) between CO_2 and crude oil (American Petroleum Institute gravity 38). The initial oil saturation was $S_O = 0.80$. Oil recovery was determined from volumetric measurements downstream of a back pressure regulator (*Equilibar HC276-5*) at ambient conditions. The injected CO_2 was exposed to the inlet end face for 5 days before the injection rate gradually increased for the subsequent 3 days, with an average rate of $6° \cdot 10^{-3}$ cm^3/min. Injection conditions were not changed during the entire test. Final oil recovery factor was $R_F = 55.0 \pm 9.2\%$ Original oil in place (OOIP), and oil was still produced (albeit at a very low rate) when the test was terminated.

Coupled fluid-rock interactions during CO_2 injection ($P_{pore} = 10$ MPa, T ambient; injection rate 0.5 cm^3/min) in Core A were studied in detail through aligned CO_2 flow PET data and rock structures CT data (see Figure 1, inset). The imaging results demonstrated that (1) the layered nature of the sample dictated the preferred flow pattern of the injected CO_2 and (2) there is a potential for CO_2 to displace oil without fracturing the tight rock. Using dynamic explicit imaging, we observed the development of a dispersed CO_2 front and accurately pinpoint the underlying cause for this behavior. The observed shape is indicative of a combination of viscous displacement and molecular diffusion, where local high-density horizontal layers reduce transverse flux. Furthermore, with access to local CO_2 flow paths, we learn that the injected CO_2 does not fracture the formation when entering the pore space to produce oil. The high oil recovery reported in the stacked system, with $R_F = 55\%$ OOIP, corroborate the second point.

3.2. Calculating the Diffusion Coefficient With PET

We use a fractured sandstone core rather than a shale sample as we here wish to emphasize the use of CO_2 tracking in the determination of D_i and not attempt an investigation of validity of Fickian diffusion in shale. Explicit CO_2 tracking was utilized in fractured, high-permeable ($\phi = 0.22$ and $K = 1.2$ D) Bentheim sandstone to determine an effective diffusion coefficient directly from PET CO_2 tracking data (Figure 2) during miscible CO_2 flow ($P = 8.3$ MPa, $T = 25$°C, and $Q = 0.15$ cm^3/min). The fracture was held open with a constant aperture of 0.5 mm using a spacer to assure a high conduit flow path to limit viscous forces. Transverse CO_2 transport from the CO_2 saturated longitudinal fracture to the completely oil-saturated (n-decane) matrix occurred by molecular diffusion only. An effective diffusion coefficient (D_i) was estimated using equation (1), with D_i as a fitting parameter. With boundary conditions $C_i(0, t) = C_0$ for $t > 0$ (i.e., constant S_{CO2} at $R_D = 0.0$) and $C_i(\infty, t) = 0$ for all t (i.e., $S_{CO2} = 0$) at $R_D = [-1, 1]$ and the initial condition $C_i(x, 0) = 0$ for all x, we derived an effective CO_2 diffusion coefficient of $2.2 \cdot 10^{-8}$ m^2/s (slightly overestimated due to decreasing volume in the transverse direction of a cylindrical core plug). The diffusion coefficient varies both with temperature and pressure, in addition to rock type (due to variations in pore sizes and distribution, i.e., diffusion path tortuosity),

and the reported coefficient agrees reasonably well to other CO_2-decane diffusion coefficient ranging between 0.83 and $5.05 \cdot 10^{-9}$ m^2/s [*Eide et al.*, 2015; *Renner*, 1988; *Tenga et al.*, 2014; *Trivedi and Babadagli*, 2006], although the literature did not use the same temperature and pressure conditions and the rock type as studied in this work. The measured $^{11}CO_2$ intensity profiles deviate from equation (1) over time as the boundary condition is violated, as expected, when the CO_2 reach the outer end of the core.

4. Concluding Remarks

We demonstrate the potential to evaluate CO_2 flow and diffusion coefficient with direct, dynamic, and explicit CO_2 tracking, rather than using indirect methods, through scouting experiments with combined PET/CT imaging. In particular, access to CO_2 flow in challenging tight formations represents a scientific advancement with potentially large impact. The main advantage with PET is its high sensitivity, requiring a tracer activity as low as 10^{-12} mol/l [*Kulenkampff et al.*, 2008], which enables accurate determination of flow, even in the ultratight samples used in this work. Indeed, separate CT imaging cannot provide the same high-quality imaging, especially in low porous rocks, although recent advances are promising [*Vega et al.*, 2014]. Combined PET/CT imaging, however, provides complementary information that exceeds the imaging capability from each method separately. This approach is utilized here to study the fluid-rock interactions relevant for flow in tight formations but can be applied to a larger range of rock types and displacement processes.

Due to the short half-life of ^{11}C (20 min), injection tests must be carefully designed and planned, and $^{11}CO_2$ cannot be used to evaluate, e.g., long-term carbon capture and storage processes like cap rock integrity [*Iglauer et al.*, 2015] or geochemical effects [*Liu et al.*, 2012]. For these processes, we propose the use of ^{22}Na (half-life 2.6 years and NaCl occurs in most brines), which enables long-term evaluation CO_2-brine-shale interaction through direct PET visualization. Based on the experimental results presented herein, we report the following key observations:

1. We show for the first time explicit CO_2 flow characterization using ^{11}C nuclides to visualize and quantify dynamic, spatial CO_2 distribution in porous media. We experimentally demonstrate the benefits of a robust, decoupled imaging approach and highlight the potential of combined PET/CT imaging. In particular, access to CO_2 flow paths in ultratight rocks represents an important technical advancement, with potentially large impact to the scientific community on transport in porous media.
2. CO_2 injection for oil recovery from unconventional, ultratight formations should be considered a viable technique for the future, and we observe recovery of $R_F = 55\%$ OOIP within 4 pore volume (PV) injected in the laboratory. The oil is produced without fracturing the formation and by developing miscibility with the crude oil saturating the pore system. The substantial oil production, compared to currently reported recovery factors, coupled with capillary trapping of CO_2, provides an economical basis for CCUS in shale formations.
3. A link between local rock structures and CO_2 flow was determined by explicit CO_2 tracking in a layered, ultratight reservoir shale ($K = 0.74$ μdarcy) sample, where the flow profile was dictated by the presence of high-density layers. Diffusive transport of CO_2 in a fractured (high-permeable) sandstone sample was visualized, and an effective diffusion coefficient ($D_i = 2.2 \cdot 10^{-8}$ m^2/s) was calculated directly from the PET images. These imaging results, along with the demonstrated applicability in tight formations, show the benefits of this imaging technique for visualization and quantification of important flow properties.

Abbreviations

API	American Petroleum Institute
CCUS	Carbon capture utilization and storage
CT	Computed tomography
EOR	Enhanced oil recovery
MMP	Minimum miscibility pressure
PET	Positron emission tomography
PV	Pore volume

Nomenclature

C_i	concentration of phase *i*
C_0	surface concentration
darcy	darcy (unit for permeability: 1 darcy = $0.9863 \cdot 10^{-12}$ m^2)
D_i	molecular diffusion coefficient for phase *i*
K	absolute permeability
P_{inlet}	absolute pressure at inlet (MPa)
P_{outlet}	absolute pressure at outlet (MPa)
P_{pore}	pore pressure (MPa)
Q	injection rate (cm^3/min)
R_D	dimensionless radius
S_{CO2}	CO_2 saturation
S_g	gas saturation
S_o	oil saturation
S_{or}	residual oil saturation
S_w	water saturation
S_{wi}	initial water saturation
t	time
x	distance
X_D	dimensionless length
ϕ	porosity

Acknowledgments
The authors are indebted to the Norwegian Research Council under Climit project 200032 "In- situ imaging of CO_2 flow, storage and entrapment in subsurface aquifers and hydrocarbon," Petromaks project 200538 "Integrated Enhanced Oil Recovery in Fractured and Heterogeneous Reservoirs," and Statoil. We also acknowledge Geir-Espen Abell and Tom Christian Holm Adamsen at Centre for Nuclear Medicine and PET, Department of Radiology, Haukeland University Hospital for the operation of PET/CT scanner. The experimental data are available upon request by contacting the corresponding author.

The Editor thanks Stefan Iglauer and an anonymous reviewer for their assistance evaluating this manuscript.

References

Boutchko, R., V. L. Rayz, N. T. Vandehey, J. P. O'Neil, T. F. Budinger, P. S. Nico, J. L. Druhan, D. A. Saloner, G. T. Gullberg, and W. W. Moses (2012), Imaging and modeling of flow in porous media using clinical nuclear emission tomography systems and computational fluid dynamics, *J. Appl. Geophys.*, *76*, 74–81, doi:10.1016/j.jappgeo.2011.10.003.

Busch, A., S. Alles, Y. Gensterblum, D. Prinz, D. N. Dewhurst, M. D. Raven, H. Stanjek, and B. M. Krooss (2008), Carbon dioxide storage potential of shales, *Int. J. Greenhouse Gas Control*, *2*(3), 297–308, doi:10.1016/j.ijggc.2008.03.003.

Chu, S., and A. Majumdar (2012), Opportunities and challenges for a sustainable energy future, *Nature*, *488*, 294–303.

Eide, Ø., M. A. Fernø, Z. Alcorn, and A. Graue (2015), Visualization of carbon dioxide enhanced oil recovery by diffusion in fractured chalk, *SPE J.*, doi:10.2118/170920-PA.

Eiken, O., P. Ringrose, C. Hermanrud, B. Nazarian, T. A. Torp, and L. Høier (2011), Lessons learned from 14 years of CCS operations: Sleipner, In Salah and Snøhvit, *Energy Procedia*, *4*(0), 5541–5548, doi:10.1016/j.egypro.2011.02.541.

Emery, G. T. (1972), Perturbation of nuclear decay rates, *Annu. Rev. Nucl. Sci.*, *22*(1), 165–202, doi:10.1146/annurev.ns.22.120172.001121.

Falcone, G., and R. Harrison (2013), Deciding whether to fund either CCS or CCUS offshore projects: Are we comparing apples and pears in the North Sea? in *SPE Annual Technical Conference and Exhibition*, Society of Petroleum Engineers, New Orleans, Louisiana, doi:10.2118/166388-ms.

Fernø, M. A., J. Gauteplass, L. P. Hauge, G. E. Abell, T. C. H. Adamsen, and A. Graue (2015), Combined positron emission tomography and computed tomography to visualize and quantify fluid flow in sedimentary rocks, *Water Resour. Res.*, *51*, doi:10.1002/2015WR017130.

Hughes, J. D. (2013), Energy: A reality check on the shale revolution, *Nature*, *494*(7437), 307–308.

Iglauer, S., C. H. Pentland, and A. Busch (2015), CO_2 wettability of seal and reservoir rocks and the implications for carbon geo-sequestration, *Water Resour. Res.*, *51*, 729–774, doi:10.1002/2014WR015553.

Kulenkampff, J., M. Gründig, M. Richter, and F. Enzmann (2008), Evaluation of positron-emission-tomography for visualisation of migration processes in geomaterials, *Phys. Chem. Earth Parts A/B/C*, *33*(14–16), 937–942, doi:10.1016/j.pce.2008.05.005.

Liu, F., P. Lu, C. Griffith, S. W. Hedges, Y. Soong, H. Hellevang, and C. Zhu (2012), CO_2–brine–caprock interaction: Reactivity experiments on Eau Claire shale and a review of relevant literature, *Int. J. Greenhouse Gas Control*, *7*(0), 153–167, doi:10.1016/j.ijggc.2012.01.012.

Maucec, M. (2013), Systems and methods for determining fluid mobility in rock samples.

Middleton, R. S., J. W. Carey, R. P. Currier, J. D. Hyman, Q. Kang, S. Karra, J. Jiménez-Martínez, M. L. Porter, and H. S. Viswanathan (2015), Shale gas and non-aqueous fracturing fluids: Opportunities and challenges for supercritical CO_2, *Appl. Energ.*, *147*, 500–509, doi:10.1016/j.apenergy.2015.03.023.

Patzek, T. W., F. Male, and M. Marder (2013), Gas production in the Barnett Shale obeys a simple scaling theory, *Proc. Natl. Acad. Sci. U.S.A.*, *110*(49), 19,731–19,736.

Renner, T. A. (1988), Measurement and correlation of diffusion coefficients for CO_2 and rich-gas applications, *SPE J.*, *3*(2), 517–523.

Tenga, Y., Y. Liua, Y. Songa, L. Jianga, Y. Zhaoa, X. Zhoua, H. Zhenga, and J. Chena (2014), A study on CO_2 diffusion coefficient in n-decane saturated porous media by MRI, *Energy Procedia*, *61*, 603–606.

Trivedi, J., and T. Babadagli (2006), Efficiency of diffusion controlled miscible displacement in fractured porous media, *Transport Porous Media.*

Vega, B., A. Dutta, and A. Kovscek (2014), CT imaging of low-permeability, dual-porosity systems using high X-ray contrast gas, *Transport Porous Media*, *101*(1), 81–97, doi:10.1007/s11242-013-0232-0.

Webb, S., and K. Pruess (2003), The use of Fick's law for modeling trace gas diffusion in porous media, *Transport Porous Media*, *51*(3), 327–341, doi:10.1023/A:1022379016613.